ACS Catalysis

Research Article

pubs.acs.org/acscatalysis

Mechanism of Cobalt-Catalyzed CO Hydrogenation: 1. Methanation

Wei Chen, Robert Pestman, Bart Zijlstra, Ivo A. W. Filot, and Emiel J. M. Hensen*

Inorganic Materials Chemistry, Schuit Institute of Catalysis, Department of Chemical Engineering and Chemistry, Eindhoven University of Technology, P.O. Box 513, 5600 MB Eindhoven, The Netherlands

Supporting Information

ABSTRACT: The mechanism of CO hydrogenation to CH_4 at 260 °C on a cobalt catalyst is investigated using steady-state isotopic transient kinetic analysis (SSITKA) and backward and forward chemical transient kinetic analysis (CTKA). The dependence of CH_x residence time is determined by $^{12}CO/H_2 \rightarrow {}^{13}CO/H_2$ SSITKA as a function of the CO and H_2 partial pressure and shows that the CH_4 formation rate is mainly controlled by CH_x hydrogenation rather than CO dissociation. Backward $CO/H_2 \rightarrow H_2$ CTKA emphasizes the importance of H coverage on the slow CH_x hydrogenation step. The H coverage strongly depends on the CO coverage, which is directly related to CO partial pressure. Combining SSITKA and backward CTKA allows determining that the amount of additional CH_4 obtained during CTKA is nearly equal to the amount of CO adsorbed to the cobalt surface. Thus, under the given conditions overall barrier for CO hydrogenation to CH_4 under methanation condition is lower than the CO adsorption energy. Forward CTKA measurements reveal that O hydrogenation to H_2O is also a relatively slow step compared to CO dissociation. The combined transient kinetic data are used to fit an explicit microkinetic model for the methanation reaction. The mechanism involving direct CO dissociation represents the data better than a mechanism in which H-assisted CO dissociation is assumed. Microkinetics simulations based on the fitted parameters confirms that under methanation conditions the overall CO consumption rate is mainly controlled by C hydrogenation and to a smaller degree by O hydrogenation and CO dissociation. These simulations are also used to explore the influence of CO and H_2 partial pressure on possible rate-controlling steps.

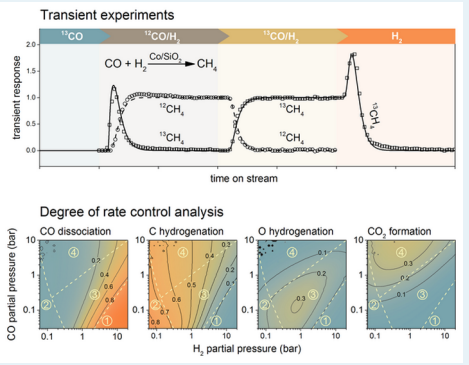

KEYWORDS: *cobalt, methanation, mechanism, SSITKA, rate-limiting step*

1. INTRODUCTION

Fischer–Tropsch synthesis is a heterogeneously catalyzed reaction whereby synthesis gas (a mixture of carbon monoxide and hydrogen) is converted into liquid fuels and chemicals.[1−3] Known since the seminal works of Franz Fischer and Hans Tropsch in the 1920s,[4,5] the Fischer–Tropsch (FT) reaction has led to large-scale industrial applications to upgrade carbonaceous feedstock such as coal and natural gas into more valuable liquid products. Supported cobalt is the preferred catalyst for the FT reaction due to its high activity, high chain-growth probability, low water–gas shift activity, and moderate deactivation.[6] A key challenge of FT technology in practice is to combine high yield of long-chain hydrocarbons with low methane selectivity. Even for methane, the simplest hydrocarbon product of the FT reaction, the exact reaction mechanism has not been resolved yet. Mechanisms proposed for the FT reaction are often based on postulated rate-determining steps leading to Langmuir–Hinshelwood equations[7] or have been developed using empiric rate equations.[8] Some of these models for the FT reaction are very sophisticated in their ability to describe important kinetic parameters such as CO consumption rate,[9] chain-growth probability,[10] and other aspects such as olefin readsorption and hydrogenation.[11,12] Nevertheless, given the complexity of the FT reaction—the large number of involved reactants, products and reaction intermediates, and the uncertainty about the reaction mechanism—there is a great need to investigate this important reaction in more detail.

Detailed insight into reaction mechanism, specifically into the way particular elementary reaction steps control reaction rate and selectivity, can be obtained by transient experiments. Transient techniques involving isotopes were developed by Happel,[13−15] Bennett[16,17] and Biloen.[18−20] Steady-state isotopic transient kinetic analysis (SSITKA) allows extracting kinetic information under steady-state conditions. The unique feature of SSITKA is that the chemical composition of the surface is not changed by the abrupt replacement of one reactant by its isotope.[21] Using this technique surface coverages and kinetic rate constants of rate-controlling steps can be determined unperturbed by changes in surface coverage. This sets SSITKA apart from chemical transient kinetic analysis techniques. Reviews of the SSITKA methodology are given by Shannon and Goodwin[22] and Ledesma et al.[23]

Received: August 14, 2017
Revised: September 24, 2017
Published: October 16, 2017

DOI: 10.1021/acscatal.7b02757
ACS Catal. 2017, 7, 8050−8060

SSITKA has already been used before to investigate the mechanism of FT catalysts.[24−27] The majority of these studies focused on methanation,[28−34] because the involved molecules are small enough to be traced online by mass spectrometry and also because the reaction network leading to methane can be formulated robustly in terms of elementary reaction steps. Regarding cobalt-catalyzed FT synthesis, it is usually assumed that CO dissociation is the rate-determining step based on the observation that the reaction order with respect to CO is negative. Matsumoto[17] and Biloen[18] made early attempts to understand the FT mechanism by transient kinetics. Another important work by Winslow and Bell combined isotopic transient kinetic analysis with in situ infrared spectroscopy to investigate the FT mechanism for supported ruthenium.[35] Winslow and Bell showed the existence of two different carbon species, one being a reactive surface intermediate and the other one involved in deactivation. These two pools of carbidic carbon have also been observed by others such as Happel et al. for nickel[15] and van Dijk et al. for cobalt[36] albeit that, different from the work of Winslow and Bell, all of the species could be hydrogenated to methane. Van Dijk et al. reported that C hydrogenation is the slow step in the mechanism of CO hydrogenation to methane by supported cobalt.[24,36] More recently, Yang et al. attributed the H_2 partial pressure dependence of the methanation reaction to the H-assisted nature of CO dissociation.[30] Den Breejen et al.[31] and Yang et al.[32] interpreted the cobalt particle size effect in terms of strongly bonded C and O atoms on small cobalt particles on the basis of SSITKA data. SSITKA investigations of promoter effects of rhenium and zinc on cobalt were reported by Yang et al.[33] and Enger et al.,[34] respectively. Recent progresses in understanding the FT mechanism by SSITKA has been reviewed by Qi et al.[37]

An important related aspect of the FT mechanism in this regard is the mode of CO dissociation. With the advent of density functional theory, the sensitivity of dissociation of molecules like CO,[38−42] NO,[43] and N_2[44,45] to the topology of metal surfaces that enclose catalytic nanoparticles has been extensively investigated. Accordingly, it has been realized that direct CO dissociation is highly likely on step-edge sites,[39−42] because the terrace sites, which dominate the surface of sufficiently large nanoparticles,[46,47] are not reactive enough. Another view is that CO activation takes place on terrace sites through an H-assisted mechanism.[30,48−52] Although it is difficult to disprove an H-assisted CO dissociation mechanism on a surface that contains adsorbed CO and H, we have recently demonstrated by isotopic exchange of a $^{12}C^{16}O/^{13}C^{18}O$ mixture that CO dissociation is fast and reversible on an empty cobalt surface.[53]

The purpose of the present work is to provide new mechanistic insight into the CO methanation reaction based on direct CO dissociation employing transient kinetic techniques. We discuss an interpretation of the H_2 pressure dependence of the methanation reaction that is different from H-assisted CO dissociation. We employ two different types of transients, a SSITKA switch involving a change in the isotopic labeling of the feed, ($^{12}CO/H_2/Ar \rightarrow {}^{13}CO/H_2/Ne$), and forward and backward CTKA transients involving Ne → CO/H_2, $Ne/H_2 \rightarrow CO/H_2$ and $CO/H_2 \rightarrow Ne/H_2$ switches. The coverage dependence of the kinetic parameters extracted from these transient measurements was evaluated by varying the CO and H_2 pressures. The obtained steady-state and transient data are modeled using the two CO dissociation mechanisms. The direct CO dissociation model that describes the data better is then used to carry out microkinetics simulations to identify the elementary reaction steps that control the CO consumption rate. An important corollary of this study will be that CO dissociation is not the rate-controlling step under methanation conditions at 260 °C. Instead, hydrogenation of O and especially of C atoms deriving from CO dissociation are identified as the slow steps. The consequences of applying different conditions (H_2/CO ratios and partial pressures) on surface composition and major rate-controlling steps will be discussed.

2. EXPERIMENTAL SECTION

Preparation and Basic Characterization. A silica-supported Co catalyst promoted by Pt was prepared by incipient wetness impregnation of SiO_2 (Shell, sieve fraction 120−250 μm, 136 m^2/g determined by BET) with an aqueous solution of $Co(NO_3)_2 \cdot 6H_2O$ (Merck, 99.99%) and $Pt(NH_3)_4 \cdot (NO_3)_2$ (Alfa Aesar, 99.995%). Pt was added as a reduction promoter. The impregnated silica was dried at 110 °C for 12 h and then calcined at 350 °C in static air for 2 h after heating to this temperature at a rate of 1 °C min^{-1}. The catalyst contained 17.1 wt % Co and 0.04 wt % Pt as determined by ICP-OES analysis (Spectroblue, AMETEK, Inc.). Co dispersion was measured by H_2-chemisorption (ASAP 2010, Micromeritics), which was carried out at 110 °C after reduction at 450 °C (heating rate 1 °C min^{-1}) for 6 h and evacuation at 470 °C for 3 h. Taking into account the degree of reduction as measured by TPR (ASAP 2920 II, Micromeritics), the particle size determined by extrapolating the straight-line portion of the adsorption isotherm to zero pressure was 19 nm. From TEM imaging (FEI Tecnai 20, LaB6, 200 kV), a volume-averaged particle size[54,55] of 15 nm was determined. The Co crystallite size determined by in situ XRD (D/max-2600, Rigaku) of the reduced catalyst by use of the Scherrer equation was 14.7 nm.

Catalytic Activity Measurements. Catalytic activity measurements were performed in a setup that is capable of transient experiments. Two identical gas-feeding units were connected to a four-way valve, which allows rapidly switching between the two feed flows. Great care was taken to keep flow perturbations minimal during switching. This was done by imposing similar pressure drop over the system between the two flow lines and the use of properly regulated mass flow controllers. A low dead-volume stainless-steel tubular reactor of 5 mm inner diameter and 80 mm bed length was used. The catalytic activity in steady state was determined by online gas chromatography (VARIAN CP-3800 equipped with TCD and FID).

Typically, 20 mg of sample diluted with SiC was loaded in the stainless-steel reactor. Prior to reaction, the sample was in situ reduced in a diluted H_2 flow (10% H_2 in Ar, 50 mL min^{-1} in total) at 450 °C using a heating rate of 2 °C min^{-1} and atmospheric pressure for 16 h. Subsequently, the sample was cooled to 260 °C in an Ar flow and the pressure was increased to 1.5 bar. Thereafter, the feed was switched to a flow containing a mixture of ^{12}CO, H_2, and Ar for 16 h to obtain steady-state conversion of the synthesis gas feed.

Transient Kinetic Experiments. Three types of transient kinetic analyses were performed, i.e., forward and backward chemical transient kinetic analysis (CTKA)[21,56−58] involving a change in the chemical composition of the gas phase (forward transient involving Ne → CO/H_2 or $Ne/H_2 \rightarrow CO/H_2$; backward transient involving $CO/H_2 \rightarrow Ne/H_2$) and a steady-

DOI: 10.1021/acscatal.7b02757
ACS Catal. 2017, 7, 8050−8060

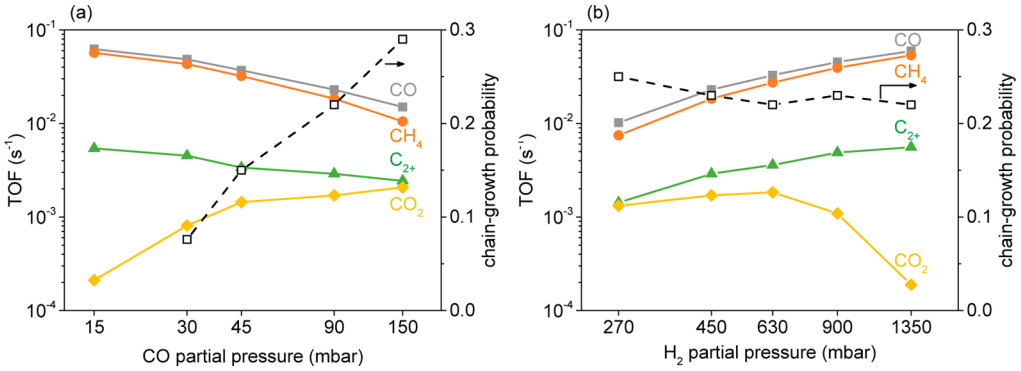

Figure 1. Turnover frequencies of CO consumption (squares), CH_4 formation (circles), C_{2+} formation (triangles), CO_2 formation (diamonds) and chain growth probability (open squares) as a function of CO partial pressure (a) and H_2 partial pressure (b). Conditions: T = 260 °C, p_{H_2} = 450 mbar at varying CO partial pressure, p_{CO} = 90 mbar at varying H_2 partial pressure.

state isotopic transient kinetic analysis (SSITKA) involving a change in the isotopic labeling of the feed ($^{12}CO/H_2/Ar \rightarrow {}^{13}CO/H_2/Ne$). In CTKA experiments, the Ne flow was used as balance to keep the total flow rate unchanged after switch. In SSITKA, the Ne was used as tracer to determine the gas-phase hold-up of the reactor. In all the experiments, an additional Ar flow was used as balance to keep H_2 partial pressure and total flow rate at 50 mL min^{-1} when the CO/H_2 ratio was varied. The concentrations of H_2 (m/z = 2), H_2O (m/z = 18), ^{12}CO (m/z = 28), ^{13}CO (m/z = 29), $^{12}CH_4$ (m/z = 15), $^{13}CH_4$ (m/z = 17), Ne (m/z = 22), and Ar (m/z = 40) were monitored by an online quadrupole mass spectrometer (GeneSys).

The CO residence time (τ) was calculated via the area under the normalized transient curves $N_{CO}(t)$, and corrected for the gas phase hold-up with the use of the Ne inert tracer.

$$\tau_{CO} = \int_0^\infty (N_{CO} - N_{Ne})dt \quad (1)$$

The CH_x (surface intermediates leading to methane) residence time was first determined in a similar way as CO, but corrected for the chromatographic effect of CO by subtracting half of the CO residence time.[18]

$$\tau_{CH_x} = \int_0^\infty (N_{CH_4} - N_{Ne})dt - \frac{1}{2}\tau_{CO} \quad (2)$$

The number of reversibly adsorbed CO and adsorbed CH_x species can be determined from the residence time and exit flow of the corresponding species. Taking into account the dispersion (the value derived from H_2-chemisorption), the surface coverage of CO and CH_x can be calculated.

$$\theta_{CO} = \tau_{CO}\frac{F_{CO}(1 - X_{CO})}{A_{Co}} \quad (3)$$

$$\theta_{CH_x} = \tau_{CH_x}\frac{F_{CO}X_{CO}S_{CH_4}}{A_{Co}} \quad (4)$$

where F_{CO} refers to the CO feed rate, A_{Co} is the number of accessible Co surface atoms determined by H_2-chemisorption, and X_{CO} and S_{CH_4} are CO conversion and CH_4 selectivity, respectively.

3. RESULTS AND DISCUSSION

Steady-State Kinetic Measurements. We first investigated the steady-state kinetics of the Co/SiO_2 catalyst at a temperature of 260 °C in order to determine reaction orders with respect to CO and H_2. The dependences of the reaction rates (expressed as turnover frequency, TOF) of CO consumption, CH_4 formation, C_{2+} formation, CO_2 formation and the chain-growth probability on CO and H_2 partial pressures are presented in Figure 1. The CO and H_2 partial pressures were varied between 15 and 150 mbar and 270−1350 mbar, respectively. At 260 °C, the main product of CO hydrogenation is CH_4. Under such methanation conditions, the chain-growth probability is low. Apparent reaction orders with respect to CO and H_2 are listed in Table 1. In line with literature,[30] the methanation rate decreases with increasing CO partial pressure, while the reverse holds true for the dependence on H_2 partial pressure. The negative reaction order with respect to CO can be interpreted in terms of a decrease in free sites needed for CO dissociation.[59] An alternative interpretation is a lack of H atoms needed for methanation. The reaction order with respect to H_2 is slightly higher than unity, implying that hydrogenation of CO or hydrogenation of C or O atoms are rate-controlling steps. We observe that the reaction order with respect to H_2 based on the CH_4 formation rate is higher than the corresponding reaction order based on the formation rate of C_{2+}-hydrocarbon products. This suggests that the H_2 partial pressure dependence at least in part originates from the rate-controlling nature of hydrogenation of C atoms, as less C hydrogenation steps for each C atom are involved in the formation of C_{2+}-hydrocarbon products than in the formation of CH_4. The rate of CO_2 formation increases with CO partial pressure and decreases with H_2 partial pressure. These

Table 1. Apparent Reaction Orders with Respect to CO and H_2 Based on CO Consumption Rate and Formation Rates of CH_4, C_{2+} and CO_2 Determined at 260°C[a]

	reaction order	
rate based on	CO[b]	H_2[c]
CO	−0.61	1.08
CH_4	−0.72	1.20
C_{2+}[d]	−0.32	0.45
CO_2	0.95	−1.09

[a]Data were acquired after 16 h time on stream. [b]p_{H_2} = 450 mbar, p_{CO} varied from 15 mbar to 150 mbar. [c]p_{CO} = 90 mbar, p_{H_2} varied from 270 mbar to 1350 mbar. [d]C_{2+} refers to all hydrocarbons containing two or more carbon atoms.

DOI: 10.1021/acscatal.7b02757
ACS Catal. 2017, 7, 8050−8060

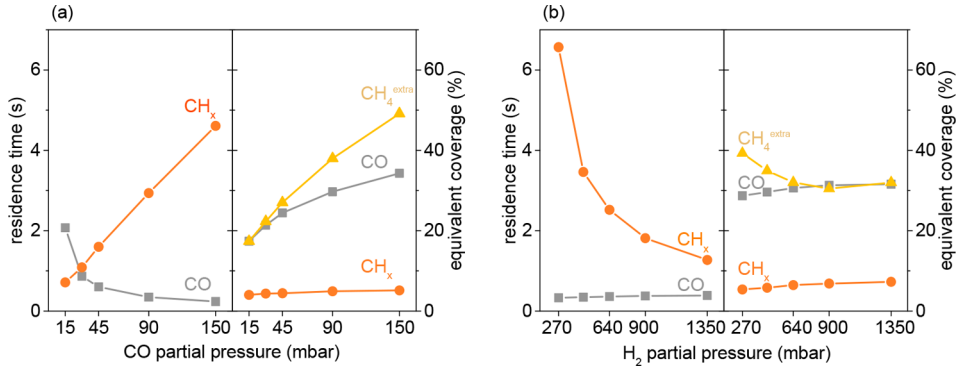

Figure 2. Residence times (left panels) and equivalent coverages (right panels) of CO (squares), CH_x (circles), and extra-CH_4 (triangles, defined in Figure 4.) as a function of CO partial pressure (a) and H_2 partial pressure (b). Conditions: T = 260 °C, p_{H_2} = 450 mbar at varying CO partial pressure, p_{CO} = 90 mbar at varying H_2 partial pressure.

dependencies point to competition of O removal pathways via CO_2 and H_2O. Although CO_2 formation cannot be neglected especially at high CO partial pressure, the dominant O removal pathway is via H_2O. It is interesting to note that the chain-growth probability only changes significantly with CO partial pressure, implying a strong influence of surface coverage on the chain-growth process. This observation will be discussed in more detailed in a companion paper that focuses on similar measurements under FT conditions at a temperature of 220 °C.

Steady-State Isotopic Transient Kinetic Analysis (SSITKA). After attaining steady state in a $^{12}CO/H_2$ mixture, the catalyst was subjected to a SSITKA switch from $^{12}CO/H_2$ → $^{13}CO/H_2$ in order to determine residence times (τ) of CO and CH_x (intermediates leading to CH_4) by use of eqs 1 and 2. Long residence time indicates low activity, and vice versa. Together with the site-normalized rates, CO and CH_x coverages can then be obtained by use of eqs 3 and 4. These residence times and coverages are plotted as a function of the CO and H_2 partial pressure in Figure 2. In good agreement with other studies,[30] a higher CO partial pressure leads to a longer residence time of CH_x. The reverse holds for changes in the H_2 partial pressure. As widely assumed in literature, CH_4 formation rate is a pseudo-first-order process with respect to the coverage of CH_x (θ_{CH_x}),[22,28−34]

$$r_{CH_4} = k'_{CH_x}\theta_{CH_x} \tag{5}$$

where k' is a pseudo-first-order rate constant and, together with eq 4, we can state that

$$k'_{CH_x} = \frac{1}{\tau_{CH_x}} \tag{6}$$

However, the pseudo-first-order assumption is not valid as the residence time also depends on the reactant partial pressure. Accordingly, we employed a more detailed analysis of the SSITKA results in which we assume that either C hydrogenation or CO dissociation is limiting the rate of CH_4 formation. The first assumption leads to decoupling of the pseudo-first-order rate constant via

$$r_{CH_4} = k'\theta_{CH_x} = k_{CH_x}\theta_H\theta_{CH_x} \tag{7}$$

where k_{CH_x} is the rate constant of hydrogenation and θ_H the H coverage. Therefore

$$k_{CH_x}\theta_H = \frac{1}{\tau_{CH_x}} \tag{8}$$

It should be noted that, at constant H_2 partial pressure, an increase in CO partial pressure will considerably reduce the H coverage, because the CO adsorbs much stronger than H_2.[60,61] On the other hand, changing H_2 partial pressure affects CO coverage less profoundly as is evident from Figure 2b. Therefore, the dependence of τ_{CHx} on either CO partial pressure or H_2 partial pressure should be largely due to a change in the H coverage, even though this cannot be exactly measured.

Alternatively, when CO dissociation is assumed to be rate-limiting, the rate can be approximated by

$$r_{CH_4} = k_{diss}\theta_v\theta_{CO} \tag{9}$$

where k_{diss} is the rate constant of CO dissociation and θ_v and θ_{CO} the surface coverages of free sites and CO, respectively. However, this assumption fails in interpreting the SSITKA observations as a function of H_2 partial pressure. We observe that CO coverage changes only slightly with varying H_2 partial pressure (Figure 2b). Considering the constant CO partial pressure, the amount of vacant sites is not expected to significantly change with increasing H_2 partial pressure. Consequently, the product of slightly changed θ_v and θ_{CO} cannot explain the 7-fold-increase in CH_4 formation rate with increasing H_2 partial pressure from 270 mbar to 1350 mbar (Figure 1).

We therefore conclude that CH_4 formation under methanation conditions is most likely controlled by hydrogenation steps that involve H atoms rather than by a CO dissociation step that involves vacancies. We also emphasize that the surface coverage plays an important role in determining the rate-controlling steps. It is to be expected that the FT reaction will occur in a different regime as CO coverage will be higher at the typically used lower temperature. SSITKA results obtained at 260 °C (this study) show the coverage of CO, the most abundant surface species, is typically no more than 0.3, which is lower than the value obtained at FT condition in a companion paper (typically 0.4 at 220 °C) and in literature (0.48[30] and 0.45[31] at 210 °C). We should take care here, as analysis based on SSITKA alone is not able to distinguish an H-assisted CO dissociation mechanism from C hydrogenation as the rate-determining step, because both depend on the H coverage. As outlined above, we have demonstrated that direct CO

DOI: 10.1021/acscatal.7b02757
ACS Catal. 2017, 7, 8050−8060

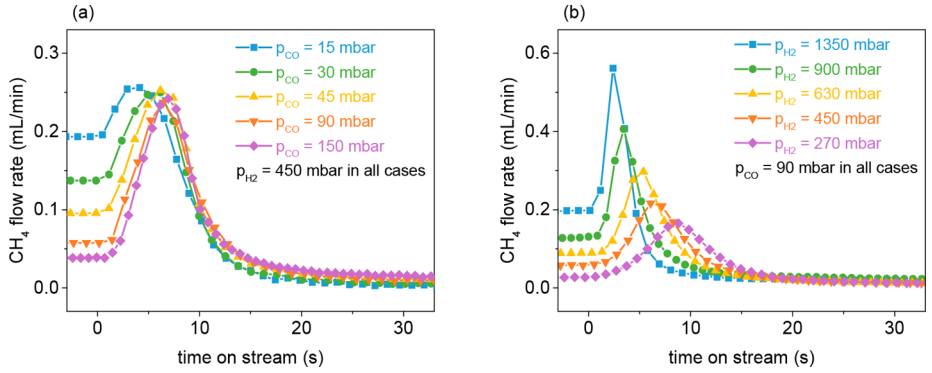

Figure 3. Backward transient at different CO partial pressures (a) and H_2 partial pressures (b) after a switch from CO/H_2 to H_2. Conditions: T = 260 °C, p_{H_2} = 450 mbar at varying CO partial pressure, p_{CO} = 90 mbar at varying H_2 partial pressure.

dissociation on the same Co/SiO_2 catalyst is possible and can be correlated to a minority site at the surface.[53] Therefore, the minor increase in CO coverage will significantly influence the reaction kinetics. This scenario will be discussed in a companion paper.

The SSITKA results reveal the strong influence of hydrogenation on the overall CO consumption rate. Both C and O hydrogenation should be considered. We therefore combine the results from SSITKA with those obtained in forward and backward CTKA and use them to fit a microkinetic model for CO hydrogenation to CH_4. From this analysis, we can identify rate-controlling steps.

Backward Chemical Transient Kinetic Analysis. The backward CTKA experiment comprises a $CO/H_2 \rightarrow Ne/H_2$ switch. Figure 3 shows that this switch leads to an increase in the CH_4 formation rate followed by a decline toward zero. This phenomenon was first observed for a fused iron catalyst by Matsumoto and Bennett.[17] Later, Cant et al. reported similar behavior for a Ru catalyst,[62] attributing the increased methane formation rate to increased H coverage. Biloen also observed the same for a Ru catalyst and suggested that the initial increase in rate of methane formation is due to an increasing pseudo-first-order rate constant of methane formation.[19] Kruse and co-workers discussed similar backward transient phenomena for a Co/MgO catalyst.[56−58] They interpreted these CTKA data as evidence for the CO-insertion mechanism. More recently, Ralston et al. explained cobalt particle size-dependent CTKA data in terms of structure sensitivity, i.e., lack of B_5−B sites for CO dissociation on small Co nanoparticles.[63]

The CTKA transients obtained at different CO and H_2 partial pressures are shown in Figure 3. The maximum CH_4 formation rates during the transient coincide with an optimum surface coverage ratio of vacancies, CO, CH_x, and H, of which the latter two determine the CH_4 formation rate. At constant H_2 pressure, the H coverage will depend linearly on the fraction of free sites according to the adsorption equilibrium of H_2. Accordingly, the optimum rate is achieved at optimum ratio of θ_{CH_x} and θ_H. This ratio is independent of the initial steady-state coverage of CO, but is reached later in time when the starting coverage is higher (Figure 3a). However, when the CO partial pressure is constant and the H_2 partial pressure is varied, the H_2 adsorption equilibrium will lead to increasing H coverage at higher H_2 partial pressure. This will lead to higher and earlier maximum CH_4 formation rate (Figure 3b). Evidently, the CH_4 formation rate is highly dependent on the H coverage.

Here, we combine for the first time SSITKA with backward CTKA in order to construct Figure 4. In this figure, we

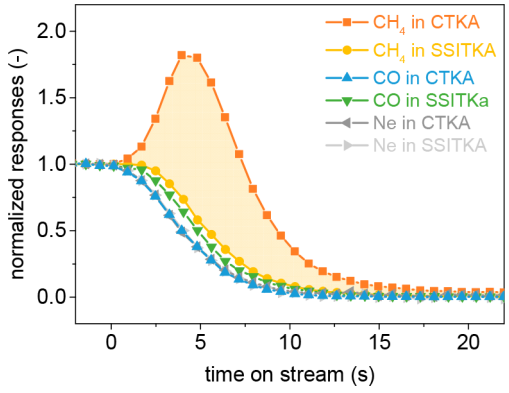

Figure 4. Normalized responses in SSITKA and backward CTKA. The extra-CH_4 is defined by as the filled area between SSITKA CH_4 (squares) and backward CTKA CH_4 (circles) responses. Steady-state conditions: T = 260 °C, p_{H_2} = 450 mbar, p_{CO} = 90 mbar.

compare CH_4 formation from two different transient experiments, viz. SSITKA and backward CTKA measurements. As only CH_4 formed during SSITKA can be assigned to CH_x species present on the surface during steady state, we define the difference as "extra-CH_4". We quantified this amount and converted it to an equivalent surface coverage by using the available Co surface area as determined by H_2-chemisorption. This surface coverage of species generating extra-CH_4 is compared to the CO coverage as determined by SSITKA. These data are displayed in Figure 2. Notably, at sufficiently high H_2/CO ratios (either at relatively low CO partial pressure or relatively high H_2 partial pressure), the amount of extra-CH_4 is equivalent to the amount of CO adsorbed on the Co surface during the steady state preceding the CTKA switch. This result indicates that the extra-CH_4 formed during the backward CTKA switch at high H_2/CO ratio can be attributed solely to conversion of adsorbed CO to methane. At low H_2/CO ratio, the amount of extra-CH_4 is slightly higher than the amount of adsorbed CO. This cannot be accounted for by higher hydrocarbon fragments present on the surface that would dissociate and hydrogenate to CH_4, because even at the lowest H_2/CO ratio the CH_4 selectivity is higher than 60% with the CH_x coverage being approximately 5% (Figure 2). As higher hydrocarbons formation typically follows an Anderson−Schulz−Flory distribution, the coverage of C_{2+}-products must

DOI: 10.1021/acscatal.7b02757
ACS Catal. 2017, 7, 8050−8060

be even lower than 5%. In this way, a pool of higher hydrocarbons cannot explain the extra-CH_4 formed relative to the amount of adsorbed CO.

Another point worth mentioning about the data in Figure 4 is that the CO signal during the SSITKA switch exhibits a delay of 1 s with respect to the inert tracer gas. This delay is caused by the adsorption/desorption equilibrium of CO in the catalyst bed, also known as the chromatographic effect. The CO response in the $CO/H_2 \rightarrow H_2$ backward CTKA switch did not exhibit this delay. Close inspection reveals that the CO signal precedes the inert tracer signal. It implies that all CO adsorbed on the Co surface is consumed and leaves the reactor predominantly as CH_4. An important corollary of this finding is that the overall barrier for CO hydrogenation to CH_4 is lower than the CO desorption energy under methanation condition.

In order to understand the deviation between the amount of extra-CH_4 and adsorbed CO, we carried out temperature-programmed hydrogenation (TPH) experiments of samples in which the flow was switched from CO/H_2 to Ar, followed by flushing in Ar for 6 h at 260 °C. After cooling to room temperature, a TPH experiments was carried out. As shown in Figure 5, there are likely two carbon-containing surface species

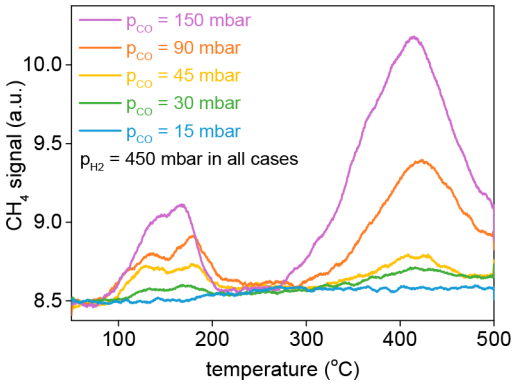

Figure 5. TPH profiles of the catalysts subjected to the methanation reaction at 260 °C for 16 h time on stream followed by an Ar purge at 260 °C for 6 h. The partial pressures presented in the graph relate to the reaction feed before the H_2 purge.

that are hydrogenated at relatively low temperature, which is below 220 °C. The data show that this carbon pool is not present at high H_2/CO ratio, but is formed in increasing amounts when the H_2/CO ratio is lowered. The nature of these carbon-containing surface intermediates remains unclear, but a particular property is that they can only be hydrogenated at sufficiently high H coverage as occurs during TPH and during the backward CTKA. Clearly, the surface will also contain even less-reactive C species as demonstrated by the reduction feature above 300 °C. Similar observations have been reported by Winslow and Bell.[35] Flushing a working Ru catalyst in He followed by temperature-programmed reduction in D_2 led to two CD_4 peaks designated as C_α and C_β, which are assigned to reactive intermediate and less reactive species causing deactivation, respectively.

Forward Chemical Transient Kinetic Analysis. We use forward CTKA to distinguish between rates of C and O hydrogenation. As the H coverage during methanation is high, both C and O hydrogenation reactions are fast. It is thus difficult to differentiate between the rates of these two reactions. Therefore, we decreased the H_2 partial pressure (200 mbar) and increased CO partial pressure (200 mbar) to amplify differences in C and O hydrogenation. The results of the forward CTKA switch are given in Figure 6. For these

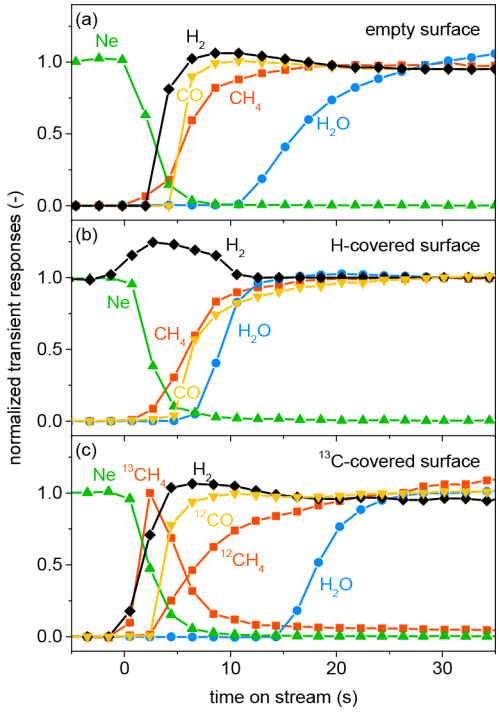

Figure 6. Forward transient on the initially empty cobalt surface (a), the H-covered surface (b), and the ^{13}C precovered surface (c). The signal intensities are normalized based on the flow rate before and after the gas switch. Steady-state conditions: T = 260 °C, p_{H_2} = 200 mbar, p_{CO} = 200 mbar.

measurements, we analyzed both CH_4 and H_2O as primary products. Analyzing H_2O during transient measurements is a challenge, because H_2O will relatively strongly interact with various parts of the setup outside the catalyst bed (mainly with the stainless-steel capillary). Accordingly, we carefully established the systematic delay due to these nonspecific interactions (see the Supporting Information). The H_2O delay values discussed below have been corrected for this systematic delay, as well as the delay caused by the chromatographic effect of CO. As before, the CH_4 delay has also been corrected for the chromatographic effect of CO.

As a reference case, we performed the forward CTKA switch on an empty cobalt surface. We obtained this state by flushing the in situ reduced Co catalyst in Ar for 2 h, followed by cooling to reaction temperature in Ar. The forward transient involved an $Ar/Ne \rightarrow H_2/CO$ switch. Figure 6a shows that CH_4 formation was delayed 2.5 s with respect to Ne, while H_2O was delayed approximately 6.5 s with respect to Ne. The specific evolution of the CH_4, H_2O, and H_2 signals also evidence that H_2 is more rapidly consumed for hydrogenation of C toward CH_4 on an initially empty cobalt surface.

The same transient experiment was also performed on a catalyst that was precovered by H_2 followed by a $H_2/Ne \rightarrow CO/H_2$ switch. In this case, the H coverage before the switch is much higher than that at reaction condition. The corresponding results in Figure 6b show a shorter H_2O delay of 0.5 s, while the decrease in the CH_4 delay (2 s) is less pronounced. This comparison implies that the H_2O delay on an empty surface is

DOI: 10.1021/acscatal.7b02757
ACS Catal. 2017, 7, 8050−8060

caused by a lack of adsorbed H, and that the O hydrogenation profits more from higher H coverage than C hydrogenation.

We also carried out an experiment in which we precovered the surface with ^{13}C atoms by exposure to ^{13}CO flow at 260 °C for 0.5 h, followed by Ar flushing to remove adsorbed ^{13}CO. As demonstrated earlier, this procedure results in the deposition of C atoms on the Co surface.[64,65] As shown in Figure 6c, the forward transient Ar/Ne → H_2/CO of this ^{13}C atom precovered surface results in a significant longer H_2O delay of 10 s, 3.5 s longer than on the empty surface and 9.5 s longer than on the H precovered surface. This increase in H_2O delay is caused by two factors. On one hand, since the surface was partially covered by ^{13}C deposits, ^{12}CO adsorption and dissociation cannot proceed until a certain fraction of ^{13}C has been removed by hydrogenation. The correspondence between the H_2 and $^{13}CH_4$ signals shown in Figure 6b represents the strong dependence of C hydrogenation on H coverage. On the other hand, the preadsorbed ^{13}C deceases H coverage. In line with the observation that an increase in H coverage effectively shortens the H_2O delay, the extra consumption of adsorbed H atoms caused by hydrogenation of precovered ^{13}C results in a longer H_2O delay with respect to $^{12}CH_4$ on a ^{13}C precovered cobalt surface (6 s) as compared to the empty surface (4 s). We stress that the competition between C and O hydrogenation is partially due to the low H_2/CO ratio in this case. The findings above also suggest that the strong dependence of H_2O formation on the H coverage significantly contributes to the reaction order with respect to H_2.

Microkinetic Modeling. A common approach to distinguish mechanisms is to fit steady-state catalytic data to a microkinetic model based on a mechanism consisting of elementary reaction steps. A major limitation of transient kinetic studies of CO hydrogenation is that the H coverage cannot be explicitly measured. This dependence is therefore often lumped into hydrogenation reaction rate constants. Here, we take a different approach in which we use transient data to fit a microkinetic model for CO hydrogenation involving H explicitly as a surface species. The elementary reaction steps that make up the microkinetic model for CO hydrogenation is given in Figure 7. The alternative kinetic model that involves

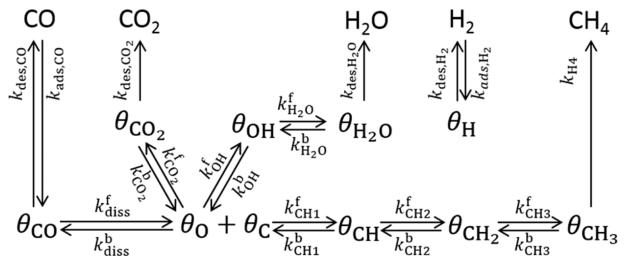

Figure 7. Schematic presentation of reaction model based on direct CO dissociation mechanism.

H-assisted CO dissociation is provided in the Supporting Information. We will first discuss the set of coupled nonlinear differential equations that describes the transient coverages of surface adsorbed species, which are the reaction intermediates. The surface coverage of CO can be described as follows:

$$\frac{d\theta_{CO}}{dt} = k_{ads,CO}p_{CO}\theta_v - k_{des,CO}\theta_{CO} - k^f_{diss}\theta_v\theta_{CO} + k^b_{diss}\theta_C\theta_O - k^f_{CO_2}\theta_{CO}\theta_O + k^b_{CO_2}\theta_v\theta_{CO_2} \quad (10)$$

The balance for CH_x species involves CH_x hydrogenation/dehydrogenation steps and also the CO dissociation for the C intermediate:

$$\frac{d\theta_C}{dt} = k^f_{diss}\theta_v\theta_{CO} - k^b_{diss}\theta_C\theta_O - k^f_{CH}\theta_H\theta_C + k^b_{CH}\theta_v\theta_{CH} \quad (11)$$

$$\frac{d\theta_{CH}}{dt} = k^f_{CH}\theta_H\theta_C - k^b_{CH}\theta_v\theta_{CH} - k^f_{CH_2}\theta_H\theta_{CH} + k^b_{CH_2}\theta_v\theta_{CH_2} \quad (12)$$

$$\frac{d\theta_{CH_2}}{dt} = k^f_{CH_2}\theta_H\theta_{CH} - k^b_{CH_2}\theta_v\theta_{CH_2} - k^f_{CH_3}\theta_H\theta_{CH_2} + k^b_{CH_3}\theta_v\theta_{CH_3} \quad (13)$$

$$\frac{d\theta_{CH_3}}{dt} = k^f_{CH_3}\theta_H\theta_{CH_2} - k^b_{CH_3}\theta_v\theta_{CH_3} - k_{CH_4}\theta_H\theta_{CH_3} \quad (14)$$

The balance for OH_x intermediates involves CO dissociation, removal of O via H_2O and CO_2:

$$\frac{d\theta_O}{dt} = k^f_{diss}\theta_v\theta_{CO} - k^b_{diss}\theta_C\theta_O - k^f_{OH}\theta_H\theta_O + k^b_{OH}\theta_v\theta_{OH} + k^f_{2OH}\theta_{OH}\theta_{OH} - k^b_{2OH}\theta_O\theta_{H_2O} - k^f_{CO_2}\theta_{CO}\theta_O + k^b_{CO_2}\theta_v\theta_{CO_2} \quad (15)$$

$$\frac{d\theta_{OH}}{dt} = k^f_{OH}\theta_H\theta_O - k^b_{OH}\theta_v\theta_{OH} - 2k^f_{2OH}\theta_{OH}\theta_{OH} + 2k^b_{2OH}\theta_O\theta_{H_2O} - k^f_{H_2O}\theta_H\theta_{OH} + k^b_{H_2O}\theta_v\theta_{H_2O} \quad (16)$$

$$\frac{d\theta_{H_2O}}{dt} = k^f_{H_2O}\theta_H\theta_{OH} - k^b_{CO_2}\theta_v\theta_{H_2O} + k^f_{2OH}\theta_{OH}\theta_{OH} - k^b_{2OH}\theta_O\theta_{H_2O} - k_{des,H_2O}\theta_{H_2O} \quad (17)$$

The balance for adsorbed CO_2 is given by

$$\frac{d\theta_{CO_2}}{dt} = k^f_{CO_2}\theta_O\theta_{CO} - k^b_{CO_2}\theta_v\theta_{CO_2} - k_{des,CO_2}\theta_{CO_2} \quad (18)$$

Finally, we provide the balance for the H surface intermediate

$$\frac{d\theta_H}{dt} = 2k_{ads,H_2}p_{H_2}\theta_v\theta_v - 2k_{des,H_2}\theta_H\theta_H - \theta_H(k^f_{CH}\theta_C + k^f_{CH_2}\theta_{CH} + k^f_{CH_3}\theta_{CH_2} + k_{CH_4}\theta_{CH_3} + k^f_{OH}\theta_O + k^f_{H_2O}\theta_{OH}) + \theta_v(k^b_{CH}\theta_{CH} + k^b_{CH_2}\theta_{CH_2} + k^b_{CH_3}\theta_{CH_3} + k^b_{OH}\theta_{OH} + k^b_{H_2O}\theta_{H_2O}) \quad (19)$$

where θ_v refers the vacant sites on surface.

An additional constraint is that the sum of all coverages is unity:

$$\theta_{CO} + \theta_C + \theta_{CH} + \theta_{CH_2} + \theta_{CH_3} + \theta_O + \theta_{CO_2} + \theta_{OH} + \theta_{H_2O} + \theta_H + \theta_v = 1 \quad (20)$$

We then used a procedure to fit this model to experimental transient CH_4 signals (comprising SSITKA, forward CTKA and

DOI: 10.1021/acscatal.7b02757
ACS Catal. 2017, 7, 8050−8060

backward CTKA). We choose transient data obtained at a high H_2/CO ratio of 15 (p_{CO} = 30 mbar, p_{H_2} = 450 mbar and T = 260 °C) so as to ensure a high CH_4 selectivity of approximately 90% and a chain-growth probability smaller than 0.1. A least-squares objective function is used as following

$$\varepsilon = \sum (f^{\text{model}}_{\text{forward}} - f^{\text{exp}}_{\text{forward}})^2 + \sum (f^{\text{model}}_{\text{SSITKA}} - f^{\text{exp}}_{\text{SSITKA}})^2 + \sum (f^{\text{model}}_{\text{backward}} - f^{\text{exp}}_{\text{backward}})^2 + w((n^{\text{model}}_{\text{CO}} - n^{\text{exp}}_{\text{CO}})^2 + (n^{\text{model}}_{\text{H}_2} - n^{\text{exp}}_{\text{H}_2})^2) \quad (21)$$

in which f denotes the normalized transient response of methane, n the reaction order, and w is a factor for giving a similar weight to the reaction orders as that to the transient data. To decrease the number of unknown variables, we introduced equilibrium constants for several surface reactions based on DFT calculations for the Co(11$\bar{2}$1) surface (Table S1 in the Supporting Information). Finally, a total of 16 rate constants were fitted. The boundary conditions and the details about the fitting procedure are discussed in the Supporting Information. The fitting results are listed in Table 2 (the results based on H-assisted CO dissociation are listed in Table S2). The good correspondence between the model and the experimental data is shown in Figure 8. The goodness of fit for the microkinetic model based on direct CO dissociation (R^2 = 0.95) is higher than the one on H-assisted CO dissociation (R^2 = 0.88). We emphasize that this criterion alone is not sufficient to rule out that a H-assisted mechanism occurs in parallel with direct CO dissociation. Therefore, we discuss the fitting results for a model based on H-assisted CO dissociation in the Supporting Information.

Table 2. Rate Constants Determined by Model Fitting

	k_f (s^{-1})	k_b (s^{-1})
adsorption/desorption		
CO + * ⇄ CO*	4.8×10^{1}	8.1×10^{-1}
H_2 + 2 * ⇄ 2 H*	7.2×10^{3}	2.5×10^{6}
H_2O* → H_2O + *	7.7×10^{1}	
CO_2* → CO_2 + *	7.7×10^{3}	
CO dissociation		
CO* + * ⇄ C* + O*	5.2×10^{-1}	7.3×10^{1}
CH_4 formation		
C* + H* ⇄ CH* + *	2.3×10^{3}	2.6×10^{1}
CH* + H* ⇄ CH_2* + *	1.9×10^{4}	2.2×10^{4}
CH_2* + H* ⇄ CH_3* + *	2.8×10^{3}	1.0×10^{2}
CH_3* + H* → CH_4 + 2 *	8.7×10^{2}	
H_2O formation		
O* + H* ⇄ OH* + *	1.7×10^{2}	9.3×10^{-3}
OH* + H* ⇄ H_2O* + *	4.7×10^{2}	1.5×10^{-1}
2 OH* ⇄ H_2O* + O*	2.8×10^{6}	2.1×10^{7}
CO_2 formation		
CO* + O* ⇄ CO_2* + *	1.1×10^{-1}	5.9×10^{-6}

Based on the fitted data, we then analyzed the different kinetic regimes of the CO hydrogenation reaction by determining the degree of rate control (DRC, see the Supporting Information). By doing so, one can identify to what extent particular elementary reaction steps control the overall CO conversion rate.[66,67] A positive DRC value ($X_{DRC,i}$) indicates that the overall reaction rate increases when the rate of elementary step i is increased. On the contrary, steps with a negative $X_{DRC,i}$ are rate-inhibiting steps that slow down the overall rate. The results are presented in Table 3 in terms of lumped DRC parameters for key reaction steps in the CO hydrogenation mechanism. A detailed list of DRC values is provided in the Supporting Information. Table 3 shows that C hydrogenation steps control the methanation reaction most. The other reaction that controls the overall rate is O hydrogenation for which we identify a X_{DRC} of 0.24. The DRC for the C−O bond scission step is only 0.15, emphasizing its weak rate-controlling nature with the hydrogenation steps. The DRC analysis based on the H-assisted CO dissociation mechanism shows qualitatively similar results (Table S3), suggesting that the conclusion of slow C and O hydrogenation at methanation conditions is independent of the CO dissociation mechanism. These conclusions are in good agreement with a recent theoretical study[68] and also the forward transient experiments in this study.

Table 3. Lumped Degree of Rate Control Values Obtained at 30 mbar CO and 450 mbar H_2

reaction	X_{DRC}
CO adsorption	-4.9×10^{-2}
H_2 adsorption	3.6×10^{-4}
CO dissociation	0.15
C hydrogenation	0.62
O hydrogenation	0.24
CO_2 formation	3.2×10^{-2}

An important conclusion from this kinetic analysis is that CO dissociation is not the rate-limiting step on cobalt at sufficiently high H_2/CO ratio and high temperature (pertaining to a relatively empty surface). Instead, the hydrogenation of the O and especially C species deriving from CO dissociation control

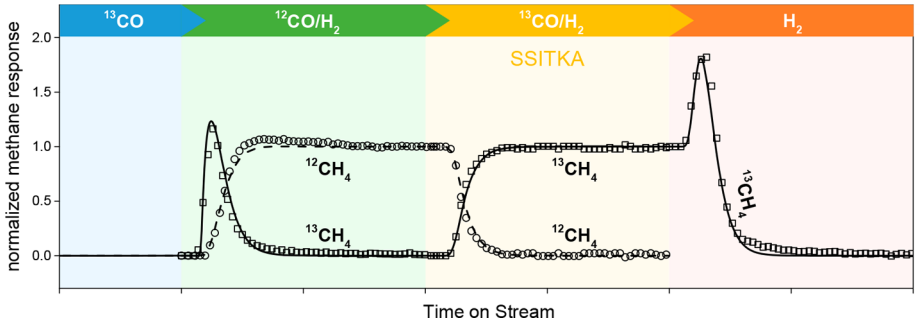

Figure 8. Combined transient data (points) and model fitting (line) based on direct CO dissociation mechanism. Steady-state conditions: T = 260 °C, p_{H_2} = 450 mbar, p_{CO} = 30 mbar.

DOI: 10.1021/acscatal.7b02757
ACS Catal. 2017, 7, 8050−8060

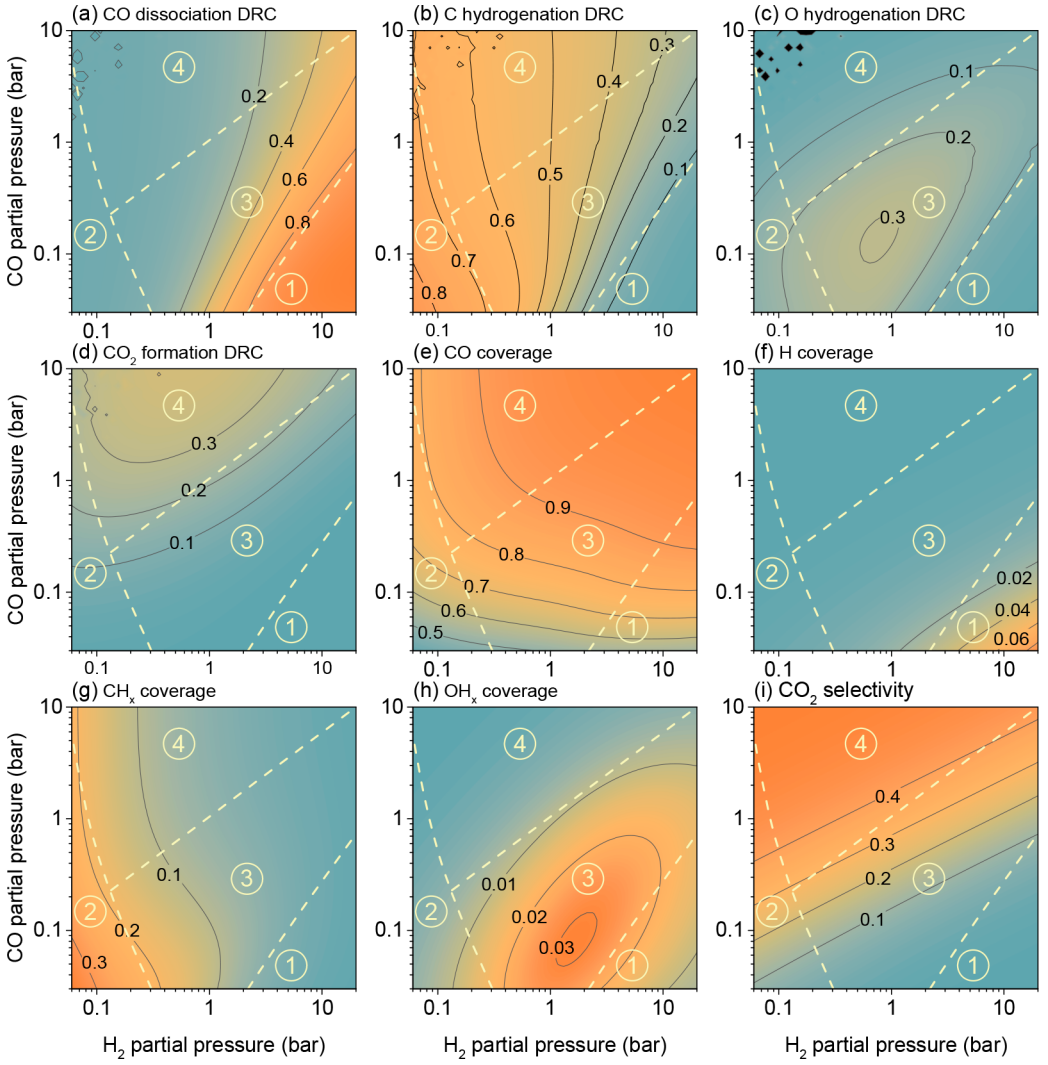

Figure 9. Degree of rate control (a-d), surface coverage (e-h) and CO_2 selectivity (i) as a function of CO and H_2 partial pressures based on a microkinetic model using parameters obtained by fitting of transient data for the methanation reaction on Co/SiO_2 (conditions: T = 260 °C, p_{H_2} = 450 mbar, p_{CO} = 30 mbar.).

the reaction rate. This finding is consistent with the experimental observation that the absolute value of H_2 reaction order for CH_4 formation is larger than that of CO reaction order, implying H_2 partial pressure affects the reaction more strongly than CO does. The influence of H_2 partial pressure on the reaction rate is larger, as the H coverage is directly related to the H_2 partial pressure; the influence of CO partial pressure is smaller as it indirectly influences the reaction by hindering H_2 adsorption.

The present work demonstrates that multiple elementary reaction steps can contribute to the rate control of the methanation reaction. The positive order with respect to H_2 is due to the rate-controlling nature of C and O hydrogenation steps. The negative CO reaction order is due to the competition between CO and H_2 adsorption, in which an increase in CO coverage decreases the H coverage that is needed for catalyzing the rate-controlling C and O hydrogenation steps.

Microkinetics Simulations. We employ the fitted microkinetic model to explore the effect of a wider range of CO and H_2 partial pressures, that is, from 0.06 to 20 bar and 0.03−10 bar, respectively. The output of these microkinetic simulations is presented in Figure 9 in the form of a DRC analysis, surface coverages, and CO_2 selectivity. Four regimes can be distinguished on the basis of the DRC values. In regime 1, the H_2 partial pressure is substantially higher than the CO partial pressure. Consequently, CO coverage is low and H coverage high. In this regime, C and O atoms derived from CO dissociation are rapidly removed as CH_4 and H_2O, respectively, and CO dissociation becomes increasingly rate-controlling with increasing H_2 pressure. Thus, C and O hydrogenation steps do not limit the CO conversion rate, but CO dissociation does. In regime 2, the surface contains a significant amount of CH_x intermediates as the lack of H atoms limits their hydrogenation. Regime 3 presents the conditions with moderate H_2/CO ratio (the diagonal lines in Figure 9 refer to a H_2/CO ratio of 2), a condition close to the FT condition. CO dissociation and C hydrogenation steps largely contribute to the overall rate control. Due to the accumulation of OH_x intermediates on the surface (Figure 9g), H_2O formation considerably controls the CO conversion rate in this regime. This is in line with recent DFT-based microkinetics simulations.[68] Meanwhile, Regime 4 refers to the lean H condition, under which the cobalt surface is fully covered by CO (Figure 9h). In this case, O is

DOI: 10.1021/acscatal.7b02757
ACS Catal. 2017, 7, 8050−8060

predominantly removed as CO_2 (Figure 9i), as the surface lacks H atoms for O hydrogenation.

These regimes provide us some insight into the different kinetic regimes one might encounter when varying the H_2/CO ratio. Notably, regime 4 is an extreme case, stemming from the higher CO_2 selectivity observed at 260 °C than at the actual FT temperature. As expected, the rate-controlling steps at conditions close to FT conditions (upper right corner in Figure 9) differ from those under methanation conditions (lower right corner in Figure 9). It appears that the very different composition of the surface adsorbed layer at lower temperature will have a significant impact on the rate-controlling nature of the different elementary reaction steps. These aspects are the focus of our companion paper which uses similar transient methodologies to interrogate the reaction mechanism of the Co/SiO_2 catalyst under conditions close to those encountered in practical FT synthesis.

CONCLUSIONS

The mechanism of CO hydrogenation to CH_4 at 260 °C on a cobalt catalyst is interrogated by different types of transient kinetic measurements including SSITKA and backward and forward CTKA. The dependence of CH_x residence time as determined by SSITKA ($^{12}CO/H_2 \rightarrow {}^{13}CO/H_2$) on CO and H_2 partial pressure indicates that the CH_4 formation rate is mainly controlled by CH_x hydrogenation rather than CO dissociation. The backward $CO/H_2 \rightarrow H_2$ CTKA emphasizes the importance of H coverage on the slow CH_x hydrogenation step. The H coverage strongly depends on the CO coverage, which is mainly determined by CO partial pressure. By combining SSITKA and backward CTKA, it is established that the additional CH_4 obtained during CTKA in comparison to SSITKA is nearly equal in amount to the amount of CO adsorbed on the cobalt surface. This implies that under the given conditions the overall barrier for CO hydrogenation to CH_4 is lower than the CO adsorption energy. Forward CTKA measurements also qualitatively show that O hydrogenation is relatively slow compared to CO dissociation. The combined transient kinetic data are captured in an explicit microkinetic model for the methanation reaction. The model fitting shows that a mechanism involving direct CO dissociation better represents the data than a mechanism in which H-assisted CO dissociation is assumed. Microkinetics simulations based on the fitted parameters show the highest DRC for C hydrogenation and lower DRC for O hydrogenation and CO dissociation at typical methanation conditions. These simulations are also used to explore different conditions depending on CO and H_2 partial pressure. This leads to four kinetic regimes in which CO consumption rate is controlled by CO dissociation, C hydrogenation, O hydrogenation, and CO_2 formation.

ASSOCIATED CONTENT

Supporting Information

The Supporting Information is available free of charge on the ACS Publications website at DOI: 10.1021/acscatal.7b02757.

(1) Correction of water transient responses; (2) validation of differential operation; (3) H-assisted CO dissociation mechanism based reaction model; (4) equilibrium constants by DFT calculation; (5) boundary conditions; (6) random sampling based global optimization approach; (7) direct CO dissociation and H-assisted CO dissociation; (8) degree of rate control determination (PDF)

AUTHOR INFORMATION

Corresponding Author

*E-mail: e.j.m.hensen@tue.nl.

ORCID

Ivo A. W. Filot: 0000-0003-1403-8379

Emiel J. M. Hensen: 0000-0002-9754-2417

Notes

The authors declare no competing financial interest.

REFERENCES

(1) Dry, M. E.; Hoogendoorn, J. C. *Catal. Rev.: Sci. Eng.* **1981**, *23*, 265−278.
(2) Dry, M. E. *Catal. Today* **2002**, *71*, 227−241.
(3) List, B. *Angew. Chem., Int. Ed.* **2014**, *53*, 8528−8530.
(4) Fischer, F.; Tropsch, H. *Ber. Dtsch. Chem. Ges. B* **1923**, *56*, 2418−2428.
(5) Fischer, F.; Tropsch, H. *Ber. Dtsch. Chem. Ges. B* **1926**, *59*, 923−925.
(6) Khodakov, A. Y.; Chu, W.; Fongarland, P. *Chem. Rev.* **2007**, *107*, 1692−1744.
(7) Yates, I. C.; Satterfield, C. N. *Energy Fuels* **1991**, *5*, 168−173.
(8) Van Der Laan, G. P.; Beenackers, A. A. C. M. *Catal. Rev.: Sci. Eng.* **1999**, *41*, 255−318.
(9) Haghtalab, A.; Nabipoor, M.; Farzad, S. *Fuel Process. Technol.* **2012**, *104*, 73−79.
(10) Wojciechowski, B. W. *Catal. Rev.: Sci. Eng.* **1988**, *30*, 629−702.
(11) Iglesia, E.; Reyes, S. C.; Madon, R. J.; Soled, S. L. *Adv. Catal.* **1993**, *39*, 221−302.
(12) Kuipers, E. W.; Vinkenburg, I. H.; Oosterbeek, H. *J. Catal.* **1995**, *152*, 137−146.
(13) Happel, J.; Kiang, S.; Spencer, J. L.; Oki, S.; Hnatow, M. A. *J. Catal.* **1977**, *50*, 429−440.
(14) Happel, J.; Suzuki, I.; Kokayeff, P.; Fthenakis, V. *J. Catal.* **1980**, *65*, 59−77.
(15) Happel, J.; Cheh, H. Y.; Otarod, M.; Ozawa, S.; Severdia, A. J.; Yoshida, T.; Fthenakis, V. *J. Catal.* **1982**, *75*, 314−328.
(16) Bennett, C. O. *Catal. Rev.: Sci. Eng.* **1976**, *13*, 121−148.
(17) Matsumoto, H.; Bennett, C. O. *J. Catal.* **1978**, *53*, 331−344.
(18) Biloen, P.; Helle, J. N.; Sachtler, W. M. H. *J. Catal.* **1979**, *58*, 95−107.
(19) Biloen, P. *J. Mol. Catal.* **1983**, *21*, 17−24.
(20) Soong, Y.; Biloen, P. *Langmuir* **1985**, *1*, 768−770.
(21) Frennet, A.; Hubert, C. *J. Mol. Catal. A: Chem.* **2000**, *163*, 163−188.
(22) Shannon, S. L.; Goodwin, J. G. *Chem. Rev.* **1995**, *95*, 677−695.
(23) Ledesma, C.; Yang, J.; Chen, D.; Holmen, A. *ACS Catal.* **2014**, *4*, 4527−4547.
(24) Van Dijk, H. A. J. *The Fischer−Tropsch synthesis A mechanistic study using transient isotopic tracing*, Ph.D. Thesis, Eindhoven University of Technology, Eindhoven, 2001.
(25) Govender, N. S. *Mechanistic study of the High- Temperature Fischer−Tropsch Synthesis using transient kinetics*, Ph.D. Thesis, Eindhoven University of Technology, Eindhoven, 2010.
(26) Fletcher, J. V. *Mechanistic Pathways of the High Temperature Fischer−Tropsch Synthesis*, Ph.D. Thesis, Eindhoven University of Technology, Eindhoven, 2016.
(27) Ledesma, C.; Yang, J.; Blekkan, E. A.; Holmen, A.; Chen, D. *ACS Catal.* **2016**, *6*, 6674−6686.
(28) Lohitharn, N.; Goodwin, J., Jr. *J. Catal.* **2008**, *257*, 142−151.
(29) Lohitharn, N.; Goodwin, J. *J. Catal.* **2008**, *260*, 7−16.
(30) Yang, J.; Qi, Y.; Zhu, J.; Zhu, Y.-A.; Chen, D.; Holmen, A. *J. Catal.* **2013**, *308*, 37−49.

DOI: 10.1021/acscatal.7b02757
ACS Catal. 2017, 7, 8050−8060

(31) Den Breejen, J. P.; Radstake, P. B.; Bezemer, G. L.; Bitter, J. H.; Frøseth, V.; Holmen, A.; Jong, K. P. d. *J. Am. Chem. Soc.* **2009**, *131*, 7197−7203.
(32) Yang, J.; Tveten, E. Z.; Chen, D.; Holmen, A. *Langmuir* **2010**, *26*, 16558−67.
(33) Yang, J.; Chen, D.; Holmen, A. *Catal. Today* **2012**, *186*, 99−108.
(34) Enger, B. C.; Frøseth, V.; Yang, J.; Rytter, E.; Holmen, A. *J. Catal.* **2013**, *297*, 187−192.
(35) Winslow, P.; Bell, A. T. *J. Catal.* **1984**, *86*, 158−172.
(36) Van Dijk, H. A. J.; Hoebink, J. H. B. J.; Schouten, J. C. *Top. Catal.* **2003**, *26*, 111−119.
(37) Qi, Y.; Yang, J.; Chen, D.; Holmen, A. *Catal. Lett.* **2015**, *145*, 145−161.
(38) De Mongeot, F. B.; Toma, A.; Molle, A.; Lizzit, S.; Petaccia, L.; Baraldi, A. *Phys. Rev. Lett.* **2006**, *97*, 056103.
(39) Shetty, S.; Jansen, A. P. J.; van Santen, R. A. *J. Am. Chem. Soc.* **2009**, *131*, 12874−12875.
(40) Shetty, S.; van Santen, R. A. *Catal. Today* **2011**, *171*, 168−173.
(41) Ge, Q.; Neurock, M. *J. Phys. Chem. B* **2006**, *110*, 15368−15380.
(42) Liu, J.-X.; Su, H.-Y.; Li, W.-X. *Catal. Today* **2013**, *215*, 36−42.
(43) Hammer, B. *Phys. Rev. Lett.* **1999**, *83*, 3681−3684.
(44) Dahl, S.; Logadottir, A.; Egeberg, R. C.; Larsen, J. H.; Chorkendorff, I.; Törnqvist, E.; Nørskov, J. K. *Phys. Rev. Lett.* **1999**, *83*, 1814−1817.
(45) Honkala, K.; Hellman, A.; Remediakis, I. N.; Logadottir, A.; Carlsson, A.; Dahl, S.; Christensen, C. H.; Norskov, J. K. *Science* **2005**, *307*, 555−8.
(46) Van Hardeveld, R.; Hartog, F. *Surf. Sci.* **1969**, *15*, 189−230.
(47) Van Helden, P.; Ciobîcă, I. M.; Coetzer, R. L. J. *Catal. Today* **2016**, *261*, 48−59.
(48) Qi, Y.; Yang, J.; Duan, X.; Zhu, Y.-A.; Chen, D.; Holmen, A. *Catal. Sci. Technol.* **2014**, *4*, 3534−3543.
(49) Ojeda, M.; Nabar, R.; Nilekar, A. U.; Ishikawa, A.; Mavrikakis, M.; Iglesia, E. *J. Catal.* **2010**, *272*, 287−297.
(50) Loveless, B. T.; Buda, C.; Neurock, M.; Iglesia, E. *J. Am. Chem. Soc.* **2013**, *135*, 6107−6121.
(51) Tuxen, A.; Carenco, S.; Chintapalli, M.; Chuang, C. H.; Escudero, C.; Pach, E.; Jiang, P.; Borondics, F.; Beberwyck, B.; Alivisatos, A. P.; Thornton, G.; Pong, W. F.; Guo, J.; Perez, R.; Besenbacher, F.; Salmeron, M. *J. Am. Chem. Soc.* **2013**, *135*, 2273−8.
(52) Mitchell, W. J.; Xie, J.; Jachimowski, T. A.; Weinberg, W. H. *J. Am. Chem. Soc.* **1995**, *117*, 2606−2617.
(53) Chen, W.; Zijlstra, B.; Pestman, R.; Hensen, E. *ChemCatChem* **2017**, DOI: 10.1002/cctc.201701203.
(54) Borodziński, A.; Bonarowska, M. *Langmuir* **1997**, *13*, 5613−5620.
(55) Carballo, J. M. G.; Yang, J.; Holmen, A.; García-Rodríguez, S.; Rojas, S.; Ojeda, M.; Fierro, J. L. G. *J. Catal.* **2011**, *284*, 102−108.
(56) Schweicher, J.; Bundhoo, A.; Kruse, N. *J. Am. Chem. Soc.* **2012**, *134*, 16135−16138.
(57) Kruse, N.; Schweicher, J.; Bundhoo, A.; Frennet, A.; Visart de Bocarmé, T. *Top. Catal.* **2008**, *48*, 145−152.
(58) Schweicher, J.; Bundhoo, A.; Frennet, A.; Kruse, N.; Daly, H.; Meunier, F. C. *J. Phys. Chem. C* **2010**, *114*, 2248−2255.
(59) Shetty, S. G.; Ciobica, I. M.; Hensen, E. J.; van Santen, R. A. *Chem. Commun.* **2011**, *47*, 9822−4.
(60) Winslow, P.; Bell, A. T. *J. Catal.* **1985**, *94*, 385−399.
(61) Toyoshima, I.; Somorjai, G. A. *Catal. Rev.: Sci. Eng.* **1979**, *19*, 105−159.
(62) Cant, N. W.; Bell, A. T. *J. Catal.* **1982**, *73*, 257−271.
(63) Ralston, W. T.; Melaet, G.; Saephan, T.; Somorjai, G. A. *Angew. Chem., Int. Ed.* **2017**, *56*, 7415−7419.
(64) Nakamura, J.; Tanaka, K.-i.; Toyoshima, I. *J. Catal.* **1987**, *108*, 55−62.
(65) Nakamura, J.; Toyoshima, I.; Tanaka, K.-i. *Surf. Sci.* **1988**, *201*, 185−194.
(66) Campbell, C. *J. Catal.* **2001**, *204*, 520−524.
(67) Stegelmann, C.; Andreasen, A.; Campbell, C. T. *J. Am. Chem. Soc.* **2009**, *131*, 8077−8082.
(68) Filot, I. A. W.; van Santen, R. A.; Hensen, E. J. M. *Angew. Chem., Int. Ed.* **2014**, *53*, 12746−12750.

DOI: 10.1021/acscatal.7b02757
ACS Catal. 2017, 7, 8050−8060